



UNIVERSIDADE ESTADUAL DE CAMPINAS
SISTEMA DE BIBLIOTECAS DA UNICAMP
REPOSITÓRIO DA PRODUÇÃO CIENTÍFICA E INTELLECTUAL DA UNICAMP

Versão do arquivo anexado / Version of attached file:

Versão do Editor / Published Version

Mais informações no site da editora / Further information on publisher's website:

<https://www.tandfonline.com/doi/full/10.1080/10916466.2021.2025072#abstract>

DOI: 10.1080/10916466.2021.2025072

Direitos autorais / Publisher's copyright statement:

©2022 by Taylor & Francis. All rights reserved.

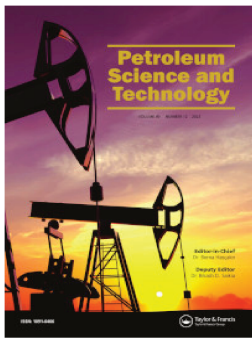
DIRETORIA DE TRATAMENTO DA INFORMAÇÃO

Cidade Universitária Zeferino Vaz Barão Geraldo

CEP 13083-970 – Campinas SP

Fone: (19) 3521-6493

<http://www.repositorio.unicamp.br>



Fault and fracture study by incorporating borehole image logs and supervised neural network applied to the 3D seismic attributes: a case study of pre-salt carbonate reservoir, Santos Basin, Brazil

Amir Abbas Babasafari, Guilherme Furlan Chinelatto & Alexandre Campana Vidal

To cite this article: Amir Abbas Babasafari, Guilherme Furlan Chinelatto & Alexandre Campana Vidal (2022) Fault and fracture study by incorporating borehole image logs and supervised neural network applied to the 3D seismic attributes: a case study of pre-salt carbonate reservoir, Santos Basin, Brazil, *Petroleum Science and Technology*, 40:12, 1492-1511, DOI: [10.1080/10916466.2021.2025072](https://doi.org/10.1080/10916466.2021.2025072)

To link to this article: <https://doi.org/10.1080/10916466.2021.2025072>

 Published online: 07 Jan 2022.

 Submit your article to this journal [↗](#)

 Article views: 378

 View related articles [↗](#)

 View Crossmark data [↗](#)

 Citing articles: 9 View citing articles [↗](#)



Fault and fracture study by incorporating borehole image logs and supervised neural network applied to the 3D seismic attributes: a case study of pre-salt carbonate reservoir, Santos Basin, Brazil

Amir Abbas Babasafari^a , Guilherme Furlan Chinelatto^a , and Alexandre Campana Vidal^b

^aCenter for Petroleum Studies, State University of Campinas, Campinas, Sao Paulo, Brazil;

^bGeoscience Institute, State University of Campinas, Campinas, Sao Paulo, Brazil

ABSTRACT

Fractures play a significant role in the development and production phases of carbonate reservoirs. Quantitative interpretation of fractures not only enhances reservoir models but also reduces the drilling risk and optimizes well design. In this study, we attempt to predict the fracture density map by integrating well and seismic data along with maximum horizontal stress identification. To this end, we propose a workflow with a set of machine learning approaches. First, 3D seismic data is conditioned after the migration processing sequence and the main faults and horizons are interpreted. Next, a number of curvature and coherence attributes are created for a supervised neural network technique to generate new seismic-based discontinuity attribute. Using a geostatistical method to incorporate the interpreted dip and azimuth attributes from well image logs and 3D seismic discontinuity attribute, the fracture density map is predicted and the results validated with a blind well. Finally, we evaluate the strike azimuth of possible open fractures based on the stress regime analysis, from which two distinctive zones are identified. There are, however, some limitations in this study. The predicted fracture density map can be employed to build a discrete fracture network, update dual porosity and permeability estimation, and identify sweet spots.

KEYWORDS

Fracture density map; seismic-based discontinuity attribute; dip and azimuth attributes; stress regime analysis; pre-salt carbonate rocks

1. Introduction

The Brazilian pre-salt carbonate rocks of the rift and post-rift stages in the Santos Basin were deposited during the Barremian and Aptian ages. These rocks are associated with regional uplift, erosion and unconformity events, and fault activation. During this period, grabens and horsts were formed via normal and strike-slip faults within the extensional tectonic setting.

This process culminated in the distinct paleo-environmental depositional conditions resulting in a diversity of carbonate deposits, as observed in the Itapema and Barra Velha formations. These carbonate rocks exhibit a variety of pore types and a wide range of heterogeneity along with depositional and diagenetic features (Chinelatto et al. 2020).

Porosity patterns in carbonate rocks are mostly controlled by factors, such as mineral composition, biological depositional environment, and diagenetic process (Herlinger, Zambonato, and De Ros 2017). A diversity of pore types, might be the consequences of the stress regime and diagenetic process (Talebi et al. 2018). Calcite shrubstone and spherulites replace magnesium and clay minerals in the Barra Velha formation of the Santos Basin, followed by compaction, dolomitization, and dissolution, which can alter pore types such as developing fractures.

(Wright and Rodriguez 2018; Martyushev 2020). Hence, the geometry evaluation of pore types is a crucial part of reservoir characterization in carbonate fields. The importance and advantages of fracture study can be summarized as follows:

- Dual porosity estimation and updating reservoir models.
- Prediction of fluid flow and permeability, which enhance reservoir simulation models and history matching.
- Better analysis of hydrodynamic and stress regimes of fault systems and also diagenesis evaluation.
- Enhanced well planning, mud weight, and casing design to reduce the drilling risks.

The novelty of this study is to identify the distribution of faults/large fractures as the main discontinuities using the supervised neural network application and then integrate them with interpreted image logs. The borehole image tools are powerful devices for structural, sedimentological, and petrophysical evaluation that are broadly used in the oil and gas industry. These tools allow the geoscientists to obtain important geological information from the field, such as the dip and azimuths of faults, fractures, and beddings, as well as the lithological texture variation of rocks in the borehole wall and identification of vuggy zones. In addition, the acoustic and resistive borehole image logs are useful for indicating borehole breakout and drilling-induced fractures in order to analyze the regional stress regime and in-situ stress. The minimum and maximum horizontal stress orientation can be identified based on the strike azimuth of borehole breakouts and drilling-induced fractures (Talebi et al. 2018).

For the identification of faults and fractures away from the wells, 3D seismic attributes are widely used to highlight the discontinuities (Chopra

and Marfurt 2017). Many seismic attributes have been developed in the past years. The variance, chaos, semblance, similarity, curvature, and ant-tracking attributes are among the most conventional seismic attributes. These attributes search for similarity or dissimilarity of a limited number of adjacent traces in order to identify lineaments. The lineaments might be classified into faults/fractures/discontinuities, stratigraphic feature's edge, e.g., channel, or even seismic noises. Considering seismic-to-well correlation, the seismic attribute (which provides the best match with 1D borehole fracture data) is nominated for fault/fracture delineation (Boersma et al. 2020). The controversial issue is the fracture size and displacement, which are below the seismic data resolution. However, the average effective properties and cumulative effects of subsurface variations are captured in the seismic data (Babasafari et al. 2020).

The application of machine learning presents an advanced and powerful tool for identifying faults and fractures. In machine learning methods, data is trained and enables the algorithm to learn and identify the structures. The unsupervised and supervised classification techniques are applied to the seismic data to reveal subsurface geological features. Supervised learning can be utilized to detect geological bodies, discontinuities, and direct hydrocarbon indicators. In the proposed workflow, a supervised neural network method was used to identify faults and large fractures.

The other point that must be considered is the origin of discontinuities, such as local folding and regional stress. Our aim is to evaluate the stress regime-related discontinuities. In this study, we faced a number of challenges including low signal-to-noise ratio of seismic data in some areas, poor image logs at several well locations, and non-availability of pre-stack 3D seismic data.

2. Geological setting

The study area is located in the Santos Basin, southeastern Brazil (Figure 1). The main reservoirs are the Itapema and Barra Velha formations. The Barra Velha formation, a focus area in this study, comprises spherulitic limestone, wackestones and packstones, carbonate mudstones, and shrub-dominated framestones associated with reworked elements of the varied carbonate and volcanic lithofacies. This formation was deposited during the Aptian age, early Cretaceous, within a lacustrine carbonate platform (Minzoni et al. 2021). A stratigraphic column of the Santos Basin, an example of core image, and thin section photomicrograph of fractures are displayed in Figure 2. The solution-enlarged fractures are filled with silicified breccia, micrite, and bioclastic debris and might be observed in the Pre-Alagoas unconformity, between the Itapema and Barra Velha

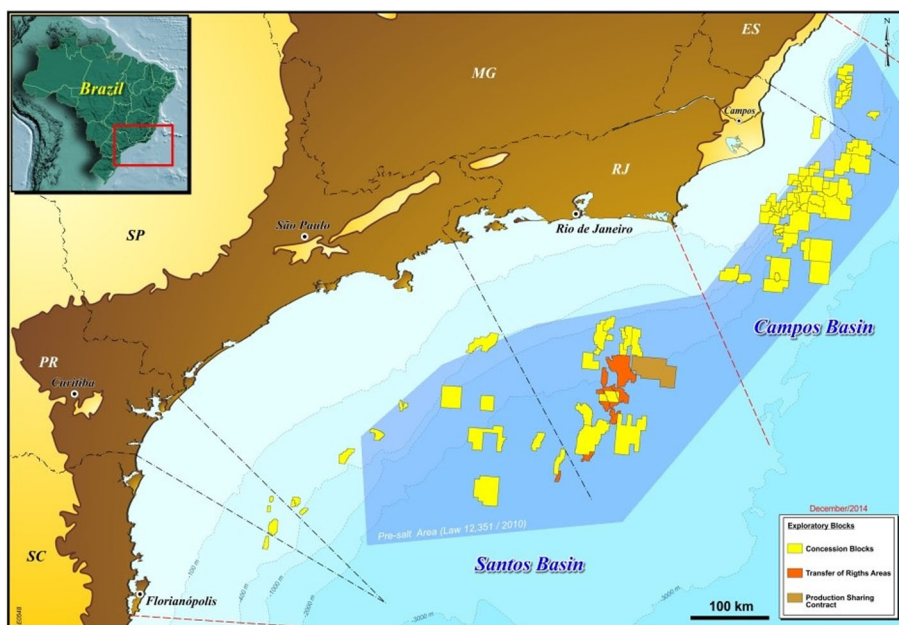


Figure 1. Santos Basin location map indicating the field of study, adapted from Gas Compression Magazine (2018).

formations, and the Intra-Alagoas unconformity, within the Barra Velha formation dividing the unit into upper and lower Barra Velha. These sub-vertical to sub-horizontal fractures are attributed to karstic fissures. The quality reservoirs are located in the carbonate mounds where potentially host karst events occur with greater intensity of fractures. The tectonic setting in the field of study is strike-slip faulting regime with normal component, which caused a number of graben and horst at the reservoir interval.

3. Methodology

3.1. Dataset and workflow

We picked a 3D pilot area as field of study in the Santos Basin. In total, 13 vertical wells (W1 to W13) were included in the selected study area. However, only eight vertical wells have conventional logs along with image logs. We employed seven wells in our workflow and one well for the blind test and validation of our result. The seismic dataset consists of a non-migrated post-stack 3D seismic volume. According to the signal-to-noise ratio, seismic data was required to be conditioned after the post-stack time migration sequence. The polarity of the zero phase seismic data is SEG normal. In this article, the zone of interest was upper Barra Velha. Check-shot correction was conducted to tie well markers in depth to seismic reflectors in the time domain. The proposed workflow for the delineation

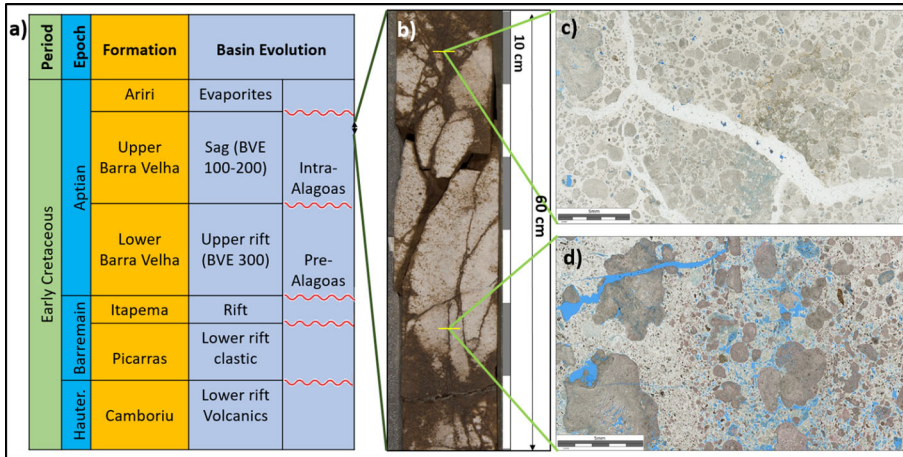


Figure 2. (a) Stratigraphic column of the Santos Basin showing the geological age, formations, and the Basin evolution, after Minzoni et al. (2021), (b) An example of core image selected from upper Barra Velha formation in the Santos Basin, the thin-sections photomicrograph illustrating (c) closed fracture filled with silicified breccia, and (d) open fracture.

of faults and fractures is displayed in Figure 3. Besides well and seismic data, the structural geology information for the stress regime analysis was incorporated in the workflow.

3.2. Faults, fractures, and borehole breakout interpretation

3.2.1. Available borehole image logs

In this work, the borehole image logs were used to interpret some structural features within the target area in the Santos Basin. The interpretation was carried out using acoustic images that were acquired with a circumferential acoustic scanning tool (CAST) from Halliburton and an ultrasonic borehole imager (UBI) from Schlumberger. Additionally, a microresistive oil mud reservoir imager (OMRI) from Halliburton and an oil base micro-imager (OBMI) from Schlumberger were also utilized as complementary tools to compare the results obtained from the acoustic image logs.

3.2.2. Dip angle and dip azimuth measurements

The structural discontinuity-related features in this study include faults (F), natural fractures (NF), drilling-induced fractures (DIF), and breakouts (BK) (Figure 4). The dip angle and dip azimuth of the mentioned structural features were measured and the faults and natural fractures were identified in the acoustic image logs based on their continuous sharp edges as well as their distinct dip and azimuth values compared to the sedimentary beddings (Figures 4a and 4b). Despite the fact that some classified fractures were interpreted as open or closed on the image logs, herein both

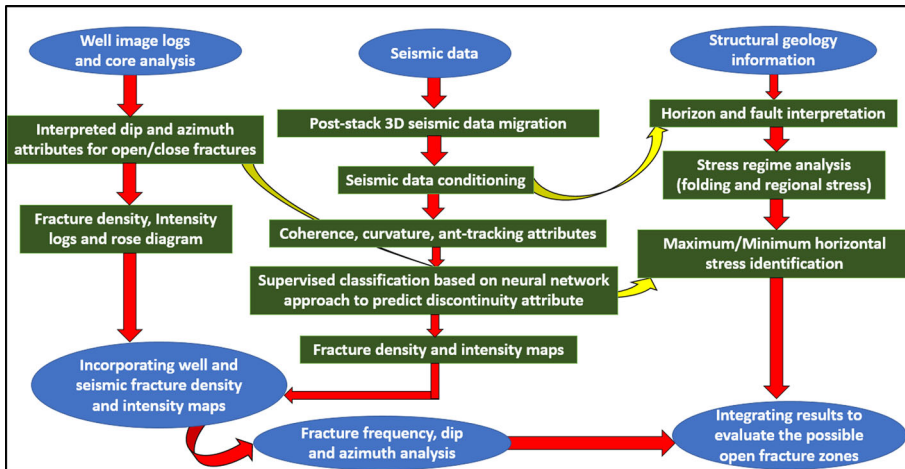


Figure 3. Proposed workflow for faults and fractures delineation.

definitions were placed as natural fractures (NF) due to the uncertainty in clearly identifying the closed fractures in the acoustic image logs.

3.2.3. Maximum and minimum horizontal stress identification

The drilling-induced fractures (DIF) and breakouts (BK) exhibit a particular distribution with specific dip and azimuth in the borehole acoustic images, which differs from the natural fractures (Figures 4c and 4d). Both drilling-induced fractures and breakouts provide essential information about the horizontal stress of the field. The drilling-induced fractures are generally generated parallel to the direction of the maximum horizontal stress of the field (Tingay, Reinecker, and Müller 2008). In contrast, the breakouts that are identified inside the greenish zones (Figure 4), with $\pm 90^\circ$ rotation relative to the orientation of drilling-induced fractures, denote the minimum horizontal stress direction in this study.

3.2.4. Fracture density calculation

The interpreted dip angle and dip azimuth of all faults and natural fractures were graphically and statistically evaluated in all wells. The properties of interpreted faults, natural fractures, drilling-induced fractures, and breakouts associated with the conventional well logs at well W6 are shown in Figure 5. A rose diagram is a helpful tool to show the frequency and orientation distribution of interpreted lineaments. The strike azimuth of fractures is measured perpendicular to their dip azimuth.

3.3. Seismic data migration, conditioning, and structural interpretation

The available post-stack 3D seismic data was not migrated. Therefore, in the first step, post-stack 3D time migration was conducted. The accuracy of

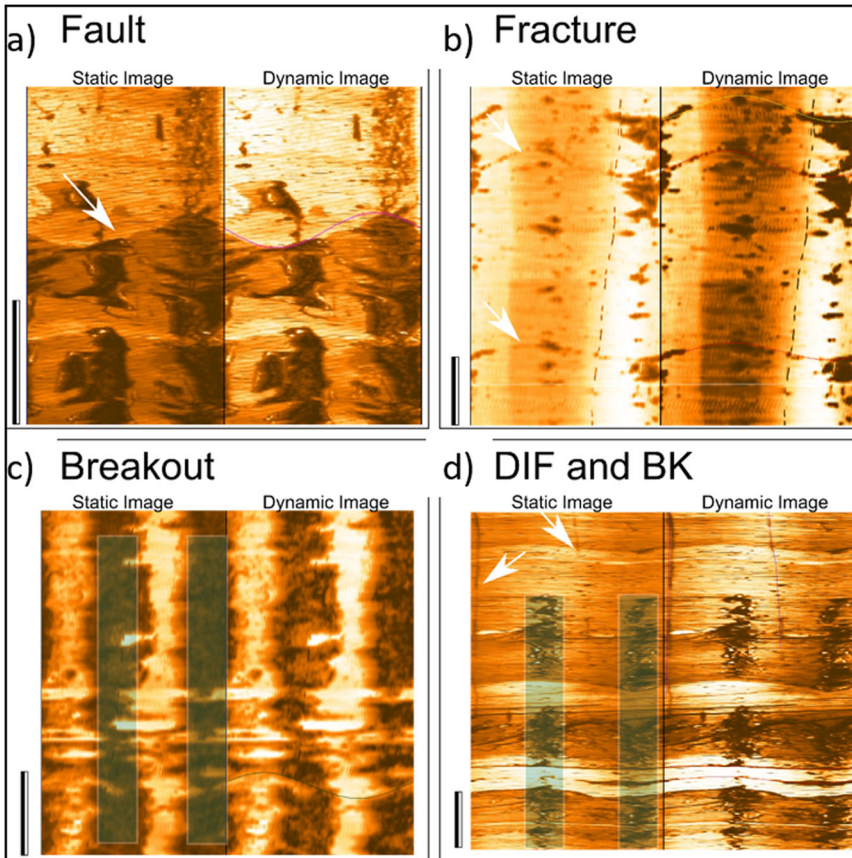


Figure 4. Interpretation of main structural discontinuity-related features using acoustic image logs. An example of (a) Fault (F), (b) Natural fractures (NF), (c) Breakouts (BK) and, (d) Drilling-induced fractures (DIF) and breakout (BK). The white arrows indicating the occurrence of F, NF, and DIF and the greenish zones showing the occurrence of BK. The scale bar in all examples corresponds to one meter in the vertical position.

seismic attributes used for faults and fractures delineation depends on the quality of input seismic data. Hence, immediately after post-stack 3D migration and before the seismic attribute study, the seismic data was conditioned to improve seismic data quality and enhance edge detection. The horizon and faults were then interpreted.

3.4. 3D Seismic attribute analysis and supervised classification

In the next step of the proposed workflow, a number of coherence and curvature attributes were generated. Next, a supervised neural network technique based on the multilayer perceptron (MLP) was employed to maximize the seismic attributes. We classified and identified fault/large fractures using a supervised classification approach by picking proper 3D seismic attributes. First, a small proportion of the entire data were visually

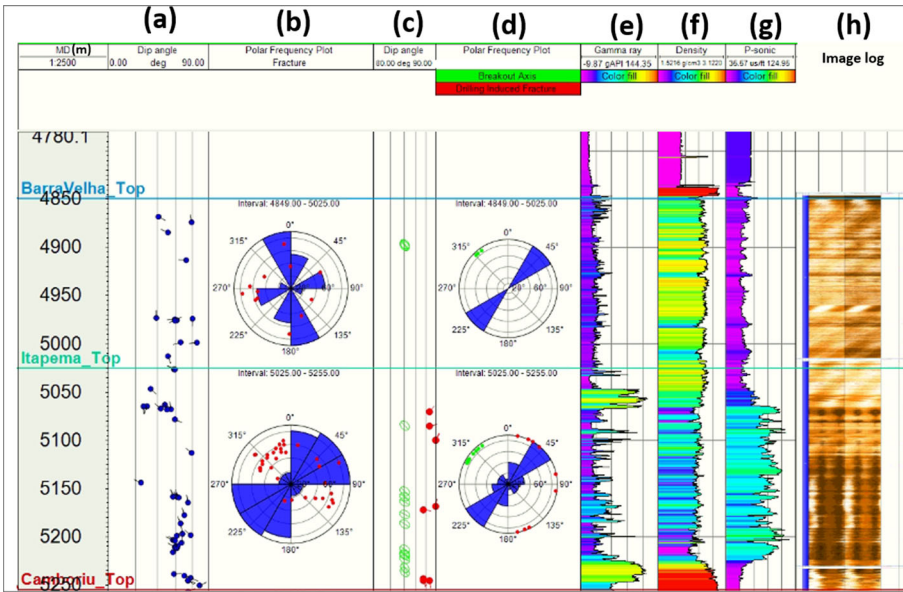


Figure 5. Interpreted fractures dip and azimuth together with the conventional well logs at well W6; (a) Dip angle of faults and natural fractures in tadpole shape, (b) Rose diagram of the fault and natural fractures showing strike azimuth, (c) Dip angle of breakout and drilling-induced fractures in tadpole shape, (d) Rose diagram of breakout and drilling-induced fractures indicating strike azimuth, (e) Gamma-ray log, (f) Density log, (g) P-sonic log, (h) Acoustic image log.

picked on the sections and time slices of 3D seismic attributes, e.g., semblance. The samples were assigned class labels; Classes 1 and 0 represent the most probable faults/fractures and non-fracture zones, respectively. Next, the chosen points were trained based on the selected attributes and finally enabled the system to learn. For this purpose, a number of 3D seismic attributes were selected as input data based on the least correlation coefficient among them to avoid bias in results via a linear classification. Eventually, the obtained non-linear relationship was applied to all samples and a 3D supervised discontinuity attribute was predicted. The discrete volume includes two labeled classes which can represent the most probable faults/fractures and non-fracture zones with space and time variations.

3.5. Calibrating seismic fracture density map with well data

FracPaQ was used in this study for the quantification of fracture patterns. The FracPaQ toolbox consists of MATLAB scripts for the analysis of fracture attributes including orientations, lengths, intensity, density and connectivity from 2D digital images, e.g., thin section photomicrographs, geological maps, aerial or satellite images (Healy et al. 2017). The trace length map, strike map, and estimated density map are some of the outputs

Table 1. The borehole image tools, depth of investigation, and the calculated fracture density at reservoir interval for each well.

Well	Borehole image tool	Total depth of investigation (m)	P10 (Number of fractures per KM)
W1	UBI	600	60
W2	CAST + OMRI	400	310
W3	CAST + OMRI	350	120
W4	CAST + OMRI	350	100
W5	UBI	330	50
W6	UBI + OBMI	500	80
W7	CAST + OMRI	450	80

of the mentioned toolbox to quantify faults and fractures. The fracture density map at the reservoir top was produced by incorporating the calculated fracture density at well locations as the primary variable and the estimated fracture density map using supervised discontinuity attribute as the secondary variable through geostatistical approach.

4. Application and discussion

The available borehole image tools for 7 wells and the total depth of investigation for dip and azimuth interpretations are illustrated in [Table 1](#). The UBI and CAST are ultrasonic tools capable of creating a 360° image of the borehole. Both provide good resolution images for structural and dip analysis, fracture identification, the borehole wall texture, and a reliable tool for breakout delineation. The OMRI and OBMI provide a microresistivity imaging in the environment of nonconductive invert emulsion mud systems. Unlike acoustic tools, the OMRI and OBMI do not provide a 360° coverage of the well. They do, however, operate in any oil or synthetic-base mud and produce high-resolution and oriented formation image. All images were processed and calibrated based on the tool characteristics, magnetic declination, and accelerometer to provide the corrected orientation of measurements.

Fractures are quantified with specific terms, such as fracture density, intensity, and porosity. Fracture density is the number of fractures per unit length, area, and volume known as P10, P20, and P30, respectively. The length of fractures per unit area is known as P21 and is referred to as the fracture intensity. The fracture density at reservoir interval was calculated for each well ([Table 1](#)). The fracture density incrementally increases toward the south and southwest study area.

In the seismic migration sequence, the seismic events are moved to their actual subsurface locations. In the area of complex geometry, such as faults and salts, the migration process helps obtain more geologically consistent images. The bow-tie features after migration sequence in seismic data processing, particularly in salt formation, were converted to syncline, as is

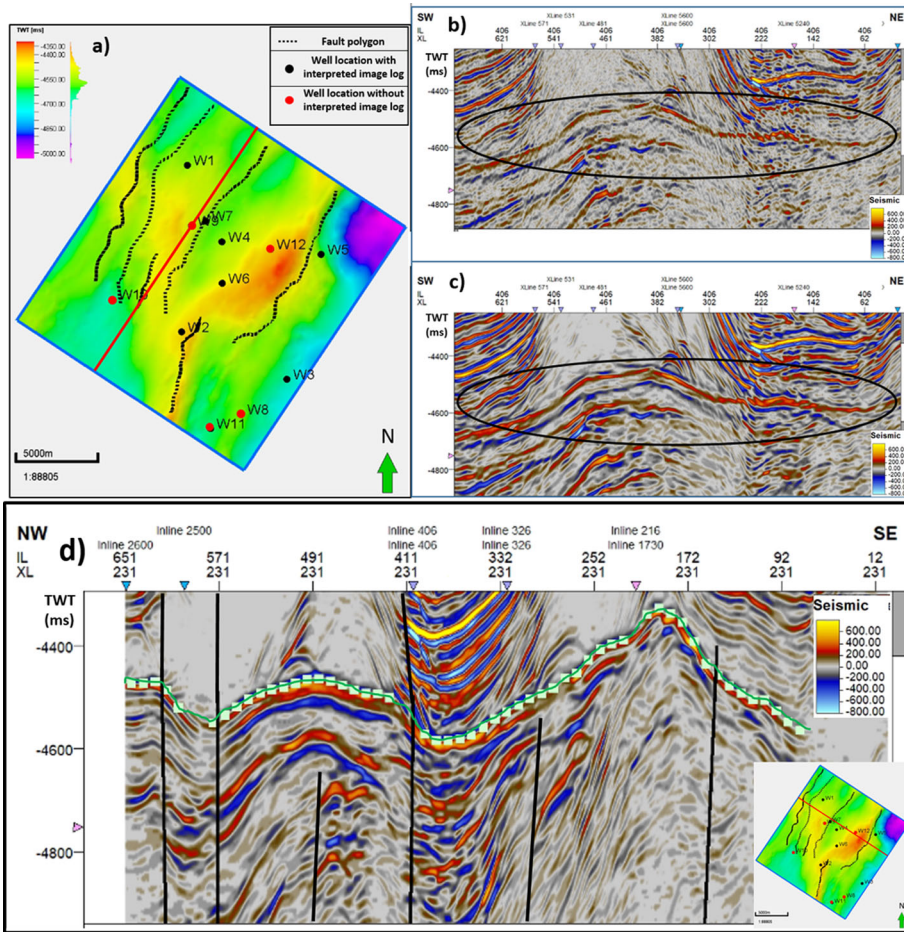


Figure 6. (a) Interpreted two-way time map of reservoir top (Barra Velha) together with the main faults polygons and location of 12 wells in the pilot study area. The seismic cross-section corresponds to the red line (b) before and (c) after dip steered median filter (DSMF). The black ellipse illustrating the reservoir interval in this study. (d) Interpreted reservoir horizon and faults shown on the seismic cross-section.

expected. The anticline and syncline-like features after migration become narrower and wider, respectively. In addition, the diffractions were collapsed after migration which can potentially mislead fault and fracture interpretation (Figures 7a and 7b).

In the seismic data conditioning step, a number of amplitude-preserved attributes were employed to clean up original seismic data. First, dip steered median filter (DSMF) was implemented after parameter optimization. Second, dip steered diffusion filter (DSDF) was performed in the same way. The first and second seismic attributes were employed to enhance signal-to-noise ratio and to highlight faults, fractures, and discontinuities on the seismic section, respectively. After check-shot correction at

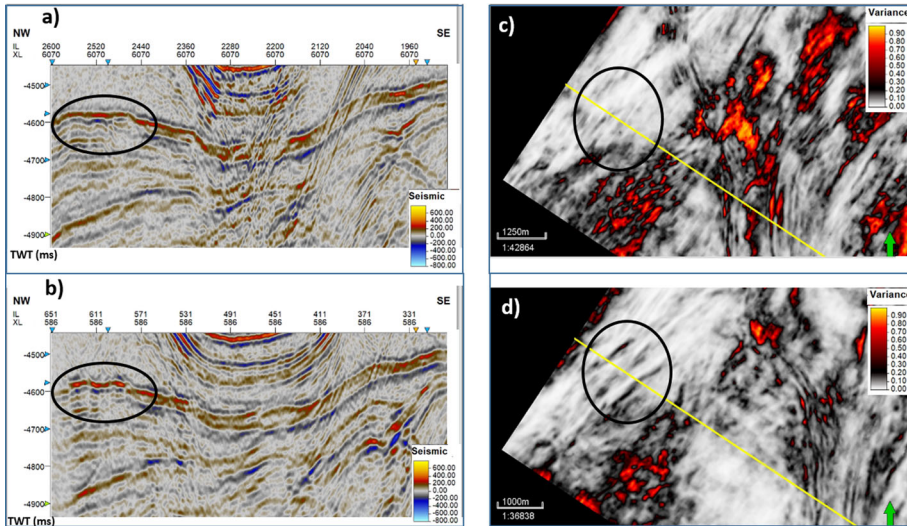


Figure 7. The seismic section corresponds to the yellow line (a) Before migration and after DSMF, (b) After migration and after DSMF, and the time slice of variance attribute applied to the seismic data (c) Before migration, (d) After migration. The black ellipse highlighting faults, fractures, and discontinuities within reservoir interval on seismic data and variance attribute after migration sequence.

well locations, the top of the upper Barra Velha was identified on the seismic reflectors. The horizon and faults were interpreted on the DSMF volume in the field of study. A total of six major fault planes were dominantly identified in the NE-SW direction. The interpreted two-way time map of reservoir top and location of 12 wells in the pilot study area are displayed in Figure 6a. The seismic data before and after applying DSMF are shown in Figures 6b and 6c, respectively. The seismic structural interpretation is illustrated in Figure 6d. The faults and discontinuities are better delineated on the seismic variance attribute after migration sequence (Figure 7).

Variance, chaos, curvature, ant-tracking, and semblance attributes were created and their ability to highlight faults, fractures, and discontinuities was evaluated. The seismic attributes were produced to reveal faults and fractures in this study (Figure 8). According to the results, the semblance attribute was selected as the most appropriate for the research objective. However, faults and fractures interpretation based on only one seismic attribute might neglect important information. Therefore, a supervised neural network technique was used. As can be seen in Figure 9a, a total of five seismic attributes were incorporated into the training model, including semblance, seismic amplitude, instantaneous frequency, curvature (most negative), and instantaneous phase. The number of seismic attributes were selected based on the least correlation coefficient among them. The supervised discontinuity attribute map and section within the reservoir interval associated with the semblance attribute are displayed in Figure 9.

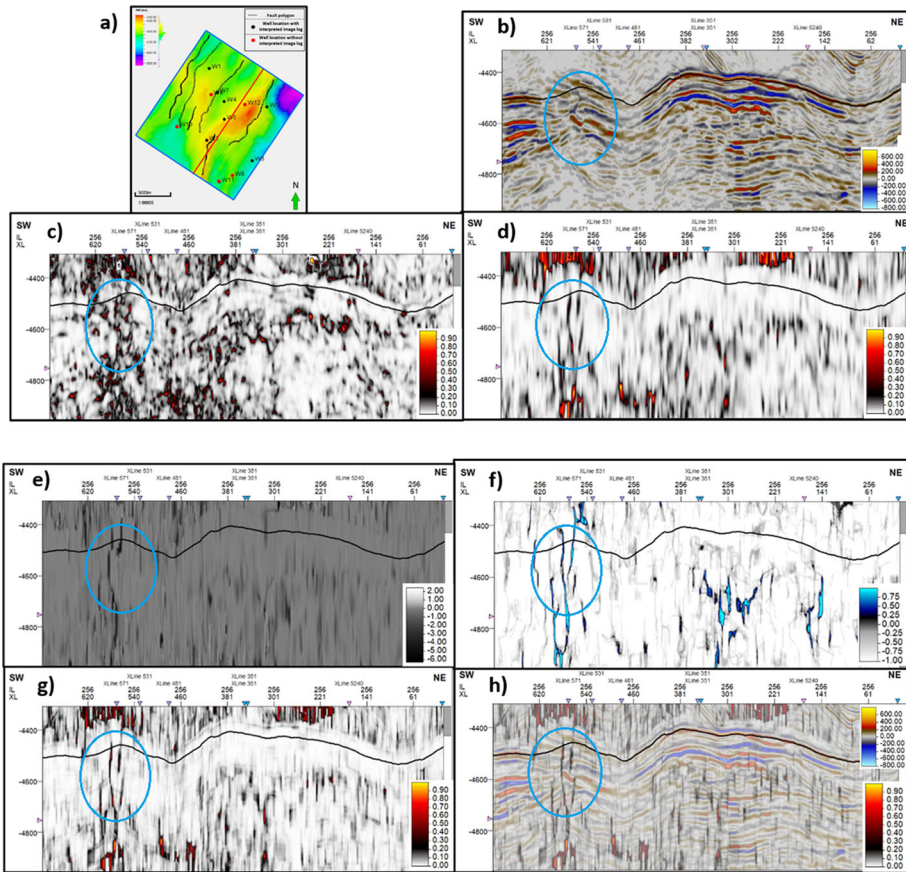


Figure 8. (a) Interpreted two-way time map of reservoir top, (b) The seismic amplitude section corresponds to the red line, and the seismic attribute sections: (c) Chaos, (d) Variance, (e) Most negative curvature, (f) Ant-tracking, (g) Semblance, (h) Seismic amplitude overlaid with semblance attribute. The black color horizon represents the Barra Velha top formation and the blue ellipse indicating faults, fractures, and discontinuities.

The fracture traces at the reservoir top were extracted from Figure 10b using the FracPaQ toolbox. After delineation of faults/fractures over the map of the Barra Velha top, some of them were excluded as they were attributed to the remaining diffractions on the seismic data. The red arrows in Figures 10a and 10b indicate the diffraction effect and chaotic zone due to poor seismic data quality on the margin of the area studied. The hand-picked lineaments were interpreted over the discontinuity attribute map that is shown in blue traces in Figure 10c. The most probable fault/fracture traces were considered in the fracture density estimation (Figure 10d). As discussed in the methodology section, the fracture density map extracted from seismic data was calibrated with fracture density values at well locations. Figure 11c shows the final map, in which the fracture density values were obtained from wells and the distribution trend of fracture density

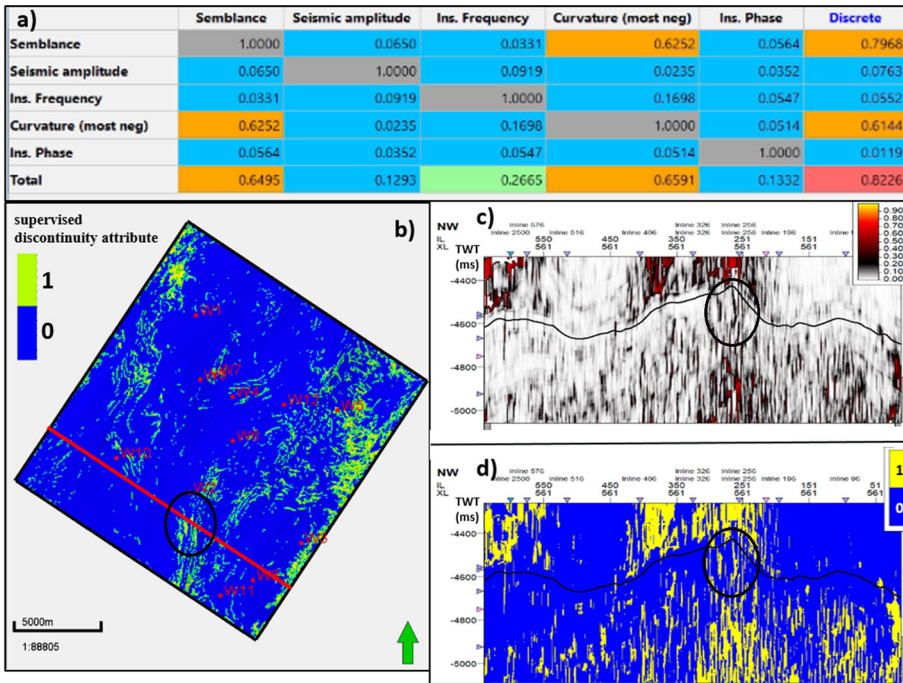


Figure 9. (a) The selected seismic attributes as input data for training in the supervised classification technique, (b) Supervised discontinuity attribute map extracted at reservoir top showing 2 classes; non-fracture (0) and fault/fracture (1), (c) Semblance attribute section, (d) Supervised discontinuity attribute section. The blue ellipse highlighting discontinuities.

away from the wells was adapted from seismic data. The result was validated with the blind well W13 shown in Figure 11c. The actual and predicted fracture density are 170 and 193, respectively. The calculated error is 13.5%. In order to estimate the fracture density map, assumptions and approximations were taken into account. Hence, the same number of fractures calculated for P10 was considered for scaling the P20 map by assuming a regular distribution of fractures per unit area.

Ladeira and Price (1981) demonstrated a direct experimental relationship between formation thickness and fracture spacing. However, if the thickness remains constant, fracture spacing varies as lithology changes. In this study, the comparison of Figures 11d and 11e shows that the increase in reservoir interval thickness in the north and northeast study area is associated with the lower number of fractures per unit area. Meanwhile, the high fracture density zones were dominantly seen in high structural locations indicated toward the south and southwest study area (Figure 11e). The strike azimuth of natural fractures at each well location is shown in Figure 12a.

Due to the poor quality of some image logs, the separation of open and closed fractures could not be implemented with a high level of confidence

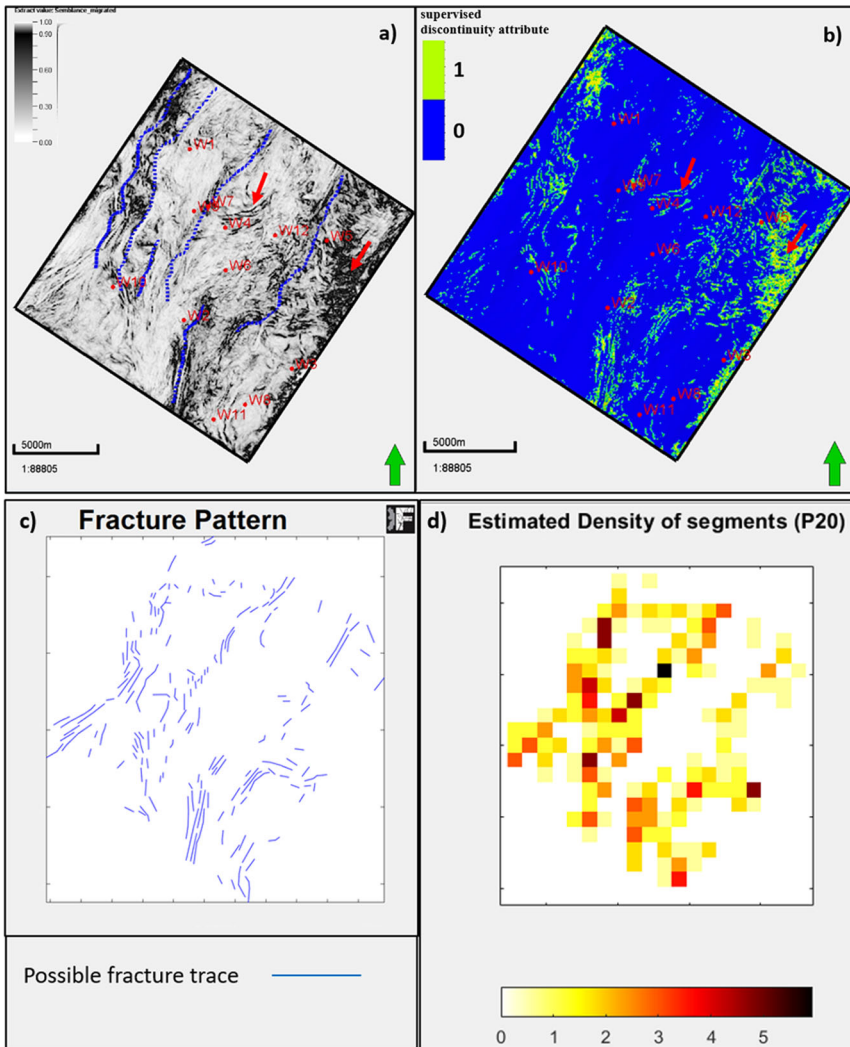


Figure 10. (a) Semblance attribute map extracted at reservoir top associated with the main faults polygons, (b) Supervised discontinuity attribute map extracted at reservoir top. Red arrows illustrating diffraction and poor signal-to-noise ratio effects. (c) The extracted fault/fracture traces at reservoir top, and (d) the estimated fracture density using FracPaQ toolbox.

(see section 3.2.2). To investigate the in-situ stress of the field with less uncertainty, borehole breakout and drilling-induced fractures were interpreted and evaluated at all seven wells. The rose diagram plot of interpreted dip angle and dip azimuth lineaments is shown in Figure 12b. Based on the strike azimuth of borehole breakout and drilling-induced fractures, the dominant minimum and maximum horizontal stress were determined in the NE-SW and NW-SE directions, respectively. The graphical representation of the strike azimuth for borehole breakout and drilling-induced fractures in this case study is illustrated in Figure 12c. The result of the

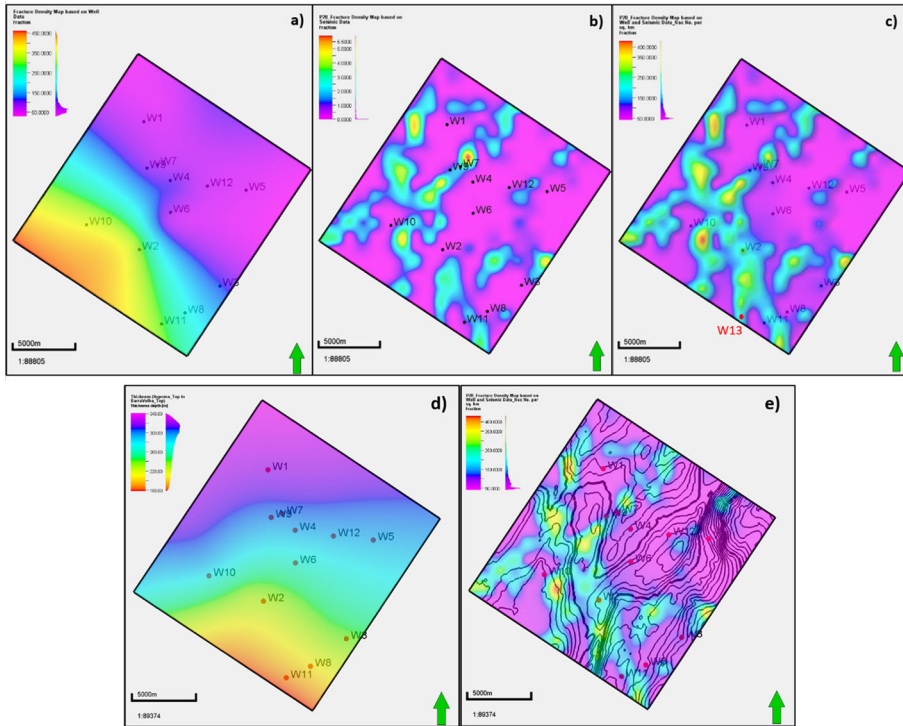


Figure 11. Fracture density map (P20) at reservoir top (a) Interpreted borehole image logs using Table 1, (b) Supervised discontinuity attribute showing in Figure 10d, and (c) Integrating Figures 11a and 11b through the geostatistical approach. The color scale is based on the fracture number per square kilometer. Well W13 used as a blind test which is indicated in Figure 11c (d) the thickness map between Barra Velha top and Itapema top formations. Interpolation is based on the well data, (e) Fracture density map (P20) at reservoir top (Figure 11c) superimposed on the structure contour map to show structural high and low in the study area. See the lower thickness corresponds to the higher fracture density indicated toward the south and southwest study area.

stress regime (Figure 12d) is consistent with the regional maximum stress direction of southern Brazil (Passarelli et al. 2011).

The main difference between the natural fractures and drilling-induced fractures is associated with their origin. The natural fractures usually occur as a result of geological process that impose stress throughout the rock, whereas drilling-induced fractures created by the regional stress of the field concentrated around a borehole and leads to the development of fractures in borehole wall while drilling. The borehole images demonstrate different traces and geometries for natural fractures and drilling-induced fractures. In image logs of vertical wells, the drilling-induced fractures exhibit sub-parallel or slightly inclined traces to the borehole axis, which are developed closely in the maximum horizontal stress direction. Moreover, when break-outs are present in the borehole images, they can help for identification of drilling-induced fractures as the breakouts are frequently generated with

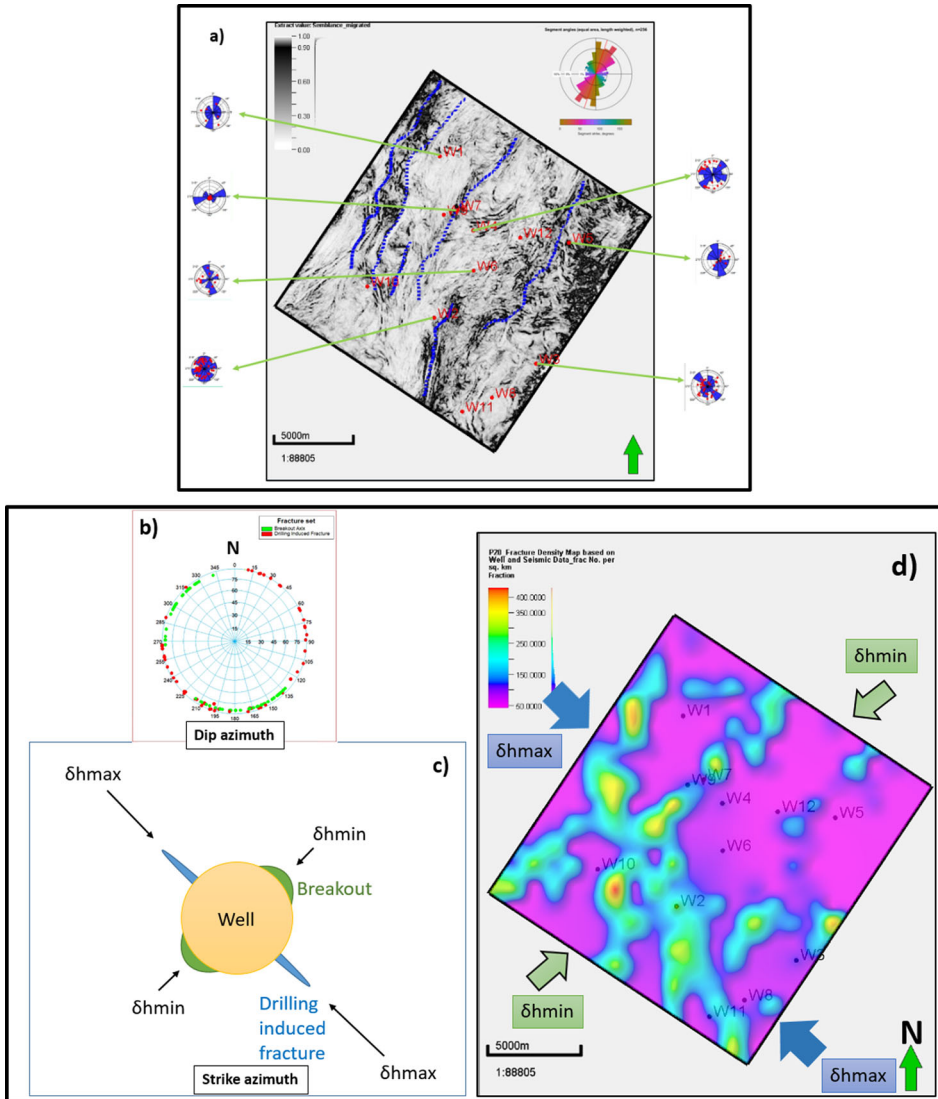


Figure 12. (a) The semblance attribute map extracted at the reservoir top associated with the main faults polygons. Rose diagrams indicate the strike azimuth of natural fractures based on the interpreted image logs at each well location and also based on the supervised discontinuity attribute map using seismic data at top of the figure, (b) Rose diagram showing dip azimuth of breakout and drilling-induced fractures based on the interpreted image logs, (c) Schematic representation of the strike azimuth for borehole breakout and drilling-induced fractures, the maximum and minimum horizontal stress is identified, after Tingay, Reinecker, and Müller (2008), (d) Fracture density map (P20) at reservoir top illustrating maximum and minimum horizontal stress in the field of study.

90° rotation relative to the orientation of drilling-induced fractures. The direction of open fractures originated from the stress regime of the field is expected to be in the same direction of maximum horizontal stress. Two

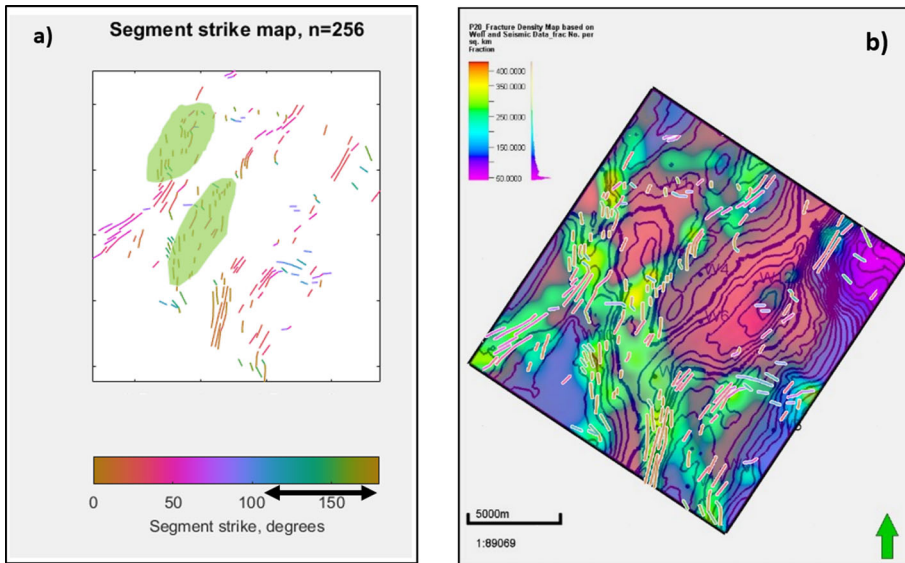


Figure 13. (a) Possible fracture traces at reservoir top. The color scale is based on the calculated strike azimuth. Two distinctive fracture zones might be caused by maximum horizontal stress of the field which can be considered as a potential area of the open fractures, (b) [Figure 11e](#) superimposed on the possible fracture traces at the reservoir top.

distinctive fracture zones following the direction of maximum horizontal stress were identified, which could potentially be the sweet spots for open fracture zones ([Figure 13](#)).

5. Uncertainties

Even though the result demonstrates an appropriate prediction of fracture density, there have been several limitations in this case study that brings uncertainties to the outcomes.

Apart from the seismic data and quality of image logs, the available seismic data was limited to post-stack narrow azimuth marine data. Therefore, the fracture azimuth study was not properly feasible. The strike azimuth of some wells is in compliance with the calculated strike azimuth of the supervised discontinuity attribute map, while a few wells seem to contradict the seismic strike azimuth trend ([Figure 12a](#)). The change in the elastic properties of seismic waves as a function of propagation direction is called seismic anisotropy. The azimuthal anisotropy can be caused by a system of fractures. Generally, for seismic fracture orientation study, the wide azimuth marine seismic data acquired by ocean-bottom seismometers (OBS) is required. In such a dataset, a particular seismic data processing is conducted to classify data into the common offset – common azimuth volumes for amplitude variation with angle and azimuth study (AVAZ) after

anisotropic velocity analysis. Furthermore, shear wave splitting analysis using multi-component seismic data is another approach for fracture azimuth study. It is worth noting that both above-mentioned techniques are not applicable in this study because the particular data is not available. Hence, the seismic anisotropy analysis was not performed.

Besides the uncertainty of the fracture azimuth study, the fracture dip interpretation must be conducted in the depth domain. The slope of faults and fractures extracted from the original seismic data is in the time domain denoted by millisecond per seismic traces distance instead of degree. Therefore, a velocity model should be built in order to convert the seismic data from time to depth domain. There is also a chance of misinterpreting some sedimentary bedding interfaces with lower slope fracture planes (less than 30 degrees) due to the quality of the image logs.

6. Conclusion

A practical workflow was conducted to predict fracture density map (P20) at reservoir top by integrating the interpreted image logs and supervised classification of seismic-based discontinuity attributes. Based on the results and stress regime analysis, the possible sweet spots for open fracture zones were identified. Two distinctive zones are located on the high fracture density and structural high toward the west and southwest study area, together with the strike azimuth orientation of interpreted lineaments, which are the same as the maximum horizontal stress orientation (NW-SE). The 3D supervised discontinuity attribute can represent the faults and natural fractures at the reservoir. However, there is uncertainty in the differentiation of open and closed fractures based on the quality of the image logs. In addition, seismic data is contaminated by amplitude attenuation and frequency absorption along with diffraction effects within the reservoir interval, whose adverse effects are inevitable on the interpreted results. Despite the limitations, the workflow can be used for other reservoir intervals. The findings of this study can potentially enhance discrete fracture network model (DFN) and dual porosity estimation in the reservoir model. Needless to say, the pore space relationship between the fracture network and karstification should be considered in the field of study. The outcomes might also be included in the geomechanical evaluation of the field for wellbore stability and mud weight design.

Acknowledgments

We gratefully acknowledge the support of EPIC – Energy Production Innovation Center, hosted by the University of Campinas (UNICAMP) and sponsored by FAPESP – São Paulo Research Foundation (2017/15736-3 and EMUs Process and/or scholarship process). We

acknowledge the support and funding from Equinor Brazil and the support of ANP (Brazil's National Oil, Natural Gas and Biofuels Agency). Acknowledgements are extended to the Center for Petroleum Studies (CEPETRO), the School of Mechanical Engineering (FEM) at UNICAMP, Dr. David Healy, Mr. Ali Rezaei Nayeh, and Ms. Luiza Mendes for their precious guidance.

Declaration of interests

The authors declare that they have no known competing financial interests or personal relationships that could have influenced the work reported in this paper.

ORCID

Amir Abbas Babasafari  <http://orcid.org/0000-0001-9904-9434>

Guilherme Furlan Chinelatto  <http://orcid.org/0000-0002-8691-5871>

References

- Babasafari, A. A., Y. Bashir, D. P. Ghosh, A. M. A. Salim, H. T. Janjuhah, S. H. Kazemeini, and M. Kordi. 2020. A new approach to petroelastic modeling of carbonate rocks using an extended pore-space stiffness method, with application to a carbonate reservoir in Central Luconia, Sarawak, Malaysia. *The Leading Edge* 39 (8):592a1–592a10. doi:10.1190/tle39080592a1.1.
- Boersma, Q., W. Athmer, M. Haege, M. Etchebes, J. Haukås, and G. Bertotti. 2020. Natural fault and fracture network characterization for the southern Ekofisk field: A case study integrating seismic attribute analysis with image log interpretation. *Journal of Structural Geology* 141:104197. doi:10.1016/j.jsg.2020.104197.
- Chinelatto, G. F., A. M. P. Belila, M. Basso, J. P. P. Souza, and A. C. Vidal. 2020. A taphofacies interpretation of shell concentrations and their relationship with petrophysics: A case study of Barremian-Aptian coquinas in the Itapema Formation, Santos Basin-Brazil. *Marine and Petroleum Geology* 116:104317. doi:10.1016/j.marpetgeo.2020.104317.
- Chopra, S., and K. J. Marfurt. 2017. Enhancing seismic discontinuity attributes with creative workflows. *AAPG Explorer* 38:20–1.
- Gas Compression Magazine. 2018. More compression for South America's Santos Basin. <https://gascompressionmagazine.com/2018/04/12/more-compression-for-south-americas-santos-basin/>
- Healy, D., R. E. Rizzo, D. G. Cornwell, N. J. Farrell, H. Watkins, N. E. Timms, E. Gomez-Rivas, and M. Smith. 2017. FracPaQ: A MATLABTM toolbox for the quantification of fracture patterns. *Journal of Structural Geology* 95:1–16. doi:10.1016/j.jsg.2016.12.003.
- Herlinger, R., E. E. Zambonato, and L. F. De Ros. 2017. Influence of diagenesis on the quality of lower cretaceous pre-salt lacustrine carbonate reservoirs from northern Campos Basin, offshore Brazil. *Journal of Sedimentary Research* 87 (12):1285–313. doi:10.2110/jsr.2017.70.
- Ladeira, F. L., and N. J. Price. 1981. Relationship between fracture spacing and bed thickness. *Journal of Structural Geology* 3 (2):179–83. doi:10.1016/0191-8141(81)90013-4.
- Martyushev, D. A. 2020. Rock stress state influence on permeability of carbonate reservoirs. *Bulletin of the Tomsk Polytechnic University, Geo Assets Engineering* 331:24–33.
- Minzoni, M., A. Cantelli, J. Thornton, and B. Wignall. 2021. Seismic-scale geometries and sequence-stratigraphic architecture of early cretaceous syn-post rift carbonate systems,

- presalt section, Brazil. *Geological Society, London, Special Publications* 509 (1):105–26. doi:10.1144/SP509-2019-78.
- Passarelli, C. R., M. A. S. Basei, K. Wemmer, O. Siga, and P. Oyhantçabal. 2011. Major shear zones of southern Brazil and Uruguay: Escape tectonics in the eastern border of Rio de La plata and Paranapanema cratons during the Western Gondwana amalgamation. *International Journal of Earth Sciences* 100 (2–3):391–414. doi:10.1007/s00531-010-0594-2.
- Talebi, H., S. A. Alavi, S. Sherkati, M. R. Ghassemi, and A. Golalzadeh. 2018. In-situ stress regime in the Asmari reservoir of the Zeloi and Lali oil fields, northwest of the Dezful embayment in Zagros fold-thrust belt, Iran. *Geosciences* 106:53–68.
- Tingay, M., J. Reinecker, and B. Müller. 2008. Borehole breakout and drilling-induced fracture analysis from image logs. *World Stress Map Project*, 1–8. <http://citeseerx.ist.psu.edu/viewdoc/download?doi=10.1.1.566.8525&rep=rep1&type=pdf>.
- Wright, P., and K. Rodriguez. 2018. Reinterpreting the South Atlantic pre-salt ‘microbialite’ reservoirs: Petrographic, isotopic and seismic evidence for a shallow evaporitic lake depositional model. *First Break* 36 (5):71–7. doi:10.3997/1365-2397.n0094.

Nomenclature

2D	Two Dimensional
3D	Three Dimensional
AVAZ	Amplitude Variation with Angle and Azimuth
BK	Breakouts
CAST	Circumferential Acoustic Scanning Tool
DSDF	Dip Steered Diffusion Filter
DSMF	Dip Steered Median Filter
DFN	Discrete Fracture Network
DIF	Drilling-Induced Fractures
F	Fault
MLP	Multi-Layer Perceptron
NF	Natural Fractures
NW-SE	Northwestern-Southeastern
OBMI	Oil Base Micro Imager
OBS	Ocean-Bottom Seismometers
OMRI	Oil Mud Reservoir Imager
SEG	Society of Exploration Geophysicists
UBI	Ultrasonic Borehole Imager
W	Well